**Metal-organic frameworks properties from hybrid density functional approximations**

# Metal-Organic Frameworks Properties from Hybrid Density Functional Approximations

Lorenzo Donà,[1] Jan Gerit Brandenburg,[2, a)] and Bartolomeo Civalleri[1, b)]
[1)] *Dipartimento di Chimica, Università di Torino and NIS (Nanostructured Interfaces and Surfaces) Centre, Via P. Giuria 7, 10125 Torino, Italy*
[2)] *Chief Science and Technology Office, Merck KGaA, Frankfurter Str. 250, 64293 Darmstadt, Germany*

(Dated: 25 February 2022)

## ABSTRACT

The chemical versatility and modular nature of Metal-Organic Frameworks (MOFs) make them unique hybrid inorganic-organic materials for several important applications. From a computational point of view, ab initio modeling of MOFs is a challenging and demanding task, in particular when the system reaches the size of gigantic MOFs as MIL-100 and MIL-101 with several thousands atoms in the unit cell. Here we show how such complex systems can be successfully tackled by a recently proposed class of composite electronic structure methods revised for solid-state calculations. These methods rely on HF/DFT hybrid functionals (i.e. PBEsol0 and HSEsol) combined with a double-zeta quality basis set. They are augmented with semi-classical corrections to take into account dispersive interactions (D3 scheme) and the basis set superposition error (gCP). The resulting methodologies, dubbed "sol-3c", are cost-effective, yet reach the hybrid functional accuracy. Here, sol-3c methods are effectively applied to predict the structure, vibrational, electronic, and adsorption properties of some of the most common MOFs. Calculations are feasible even on very large MOFs containing more than 2500 atoms in the unit cell as MIL-100 and MIL-101 with reasonable computing resources. We propose to use our composite methods for the routine In Silico screening of MOFs targeting properties beyond plain structural features.

## I. INTRODUCTION

Metal Organic Frameworks[1,2] (MOFs) represent a wide class of hybrid organic-inorganic materials composed by an inorganic clusters (also known as metal knots) interconnected by polytopic organic linkers that self-assembly in a three-dimensional, crystalline and microporous structure. During the last two decades these materials have gained considerable attention in industry and academic world thanks to their modular nature, high chemical versatility and tunability. All these features make MOFs promising materials for vast variety of applications ranging from gas storage[3] and separation[4], to (photo)catalysis[5], mechanical and chemical sensing[6], and to opto(electronics)[7,8] and drug delivery[9,10]. Another promising application area is to use the porous complexes to enable X-ray analysis of molecules that do not natively crystallize or where just few nanograms are available.[11] These crystalline sponges for structure elucidation are currently developed into a commercially available technology.[12]

From a computational point of view, theoretical modelling of MOFs is not a straightforward task due to the presence of several levels of complexity that can be summarized as:

(i) The number of synthesized and hypothetical structures is continuously increasing. For instance, more than 70 000 structures of MOFs have been recently identified in the Cambridge Structure Database[13,14] and the CoReMOF dataset of computation-ready metal-organic frameworks contains more than 100 000 structures[15].

(ii) The size of the system in terms of number of atoms and unit cell volume, varies remarkably from small MOFs containing less then 40 atoms in the unit cell (e.g. MIL-53[16]) to giant MOFs with more than 2000 atoms per unit cell (e.g. MIL-100[17], MIL-101[10], bio-MOFs[18,19]).

(iii) The intrinsic complexity of MOFs due to their modular nature with the combination of different Secondary Building Units (SBU) that leads to a large variety of framework topologies, but also to frameworks modifications (e.g interpenetration), host-guest interactions, flexibility and defects.

This scenario represents a challenge for computational studies of MOFs, but also the prediction of their physical and chemical properties is not trivial and requires a proper choice of the adopted level of theory[20]. Therefore, to tackle the structural and chemical complexity of MOFs, accurate yet cost-effective computational methods are needed.
In the last years, a family of composite electronic structure methods has been proposed.[21–25] They range from Hartree-Fock to pure and hybrid exchange correlation functionals, which are combined with small to medium Gaussian basis set and augmented with semi-classical corrections to describe London dispersion interactions at long range through the D3[26] or D4[27,28] scheme and remove the basis set superposition error (BSSE) via the gCP[29,30] method. These composite methods dubbed "3c" have been targeted to molecules and organic crystals[31] and they have been shown to provide very good results on geometric and thermochemical properties[32]

[a)] Electronic mail: j.g.brandenburg@gmx.de
[b)] Electronic mail: bartolomeo.civalleri@unito.it

but they are only partly applicable and transferable to solid-state calculations. Therefore, we recently proposed a revised version of such methods specifically designed for solid state calculations[33]. In particular, we adopted exchange-correlation functionals for solids hybridized with 25% of HF exchange and reshaped the molecular basis set to make them suitable for ionic, covalent and molecular solids, inorganic compounds and hybrid materials, such as MOFs. The new revised methods have been renamed "sol-3c"[33] to emphasize a broader range of applicability, including solids. They have also been proved to efficiently tackle large systems of up to thousands of atoms with excellent performance, even with small-scale computing resources.[34]

In this work, we show how "sol-3c" methods can be successfully applied to model various properties of MOFs, e.g. equilibrium structures, vibrational frequencies and simulated IR/Raman spectra, fundamental band gap, phase stability and adsorption of small molecules. Furthermore, we show that hybrid HF/DFT composite methods can be effectively employed to simulate very large MOFs such as the so-called giant-MOFs (i.e. MIL-100[17] and MIL-101[35]).

## II. METHODS

### A. Composite Hybrid HF/DFT

In this section we briefly recall the main ingredients of the composite hybrid HF/DFT methods which are examined in the present work. The total energy provided can be written as[32]

$$E_{\mathrm{tot}}^{\text{sol-3c}} = E_{\mathrm{tot}}^{\mathrm{DFT/basis}} + E_{\mathrm{disp}}^{\mathrm{D3}} + E_{\mathrm{BSSE}}^{\mathrm{gCP}} \tag{1}$$

$E_{\mathrm{tot}}^{\mathrm{DFT/basis}}$ denotes the total energy evaluated with the hybrid XC functional. In the present work, the theoretical methods are the global hybrid PBEsol0 functional[36] and the range-separated hybrid HSEsol functional[37]. The two methods were chosen because they were specifically devised for solids and they use 25% of exact exchange in the hybrid exchange functional, which has been shown to be a good compromise.[38] The basis is the revised def2-mSVP for PBEsol0-3c and HSEsol-3c.[22] The $E^{\mathrm{DFT/basis}}$ total energy is supplemented with a damped atom-atom two-body dispersion energy as defined in the D3 approach[26]:

$$E_{\mathrm{disp}}^{\mathrm{D3(BJ)}} = -\frac{1}{2}\sum_{AB}\sum_{n=6,8} s_n \frac{C_n^{AB}}{R_{AB}^n} f_{\mathrm{damp}}^{(n)}(R_{AB}) \tag{2}$$

Here, $C_n^{AB}$ denotes the $nth$-order dispersion coefficient (orders = 6, 8) for each atom pair AB, $R^{AB}$ is their inter-nuclear distances and $s_n$ are the order-dependent scaling factors. The rational Becke-Johnson damping function[39] has become the default in combination with D3[40]:

$$f_{\mathrm{damp}}^{(n)}(R_{AB}) = \frac{R_{AB}^n}{R_{AB}^n + (a_1 R_0^{AB} + a_2)^n} \tag{3}$$

The damping function incorporates radii for atomic pairs $R_0^{AB} = \sqrt{C_8^{AB}/C_6^{AB}}$ and functional-specific parameters $a_1$ and $a_2$ that have been refitted in the present work for the different composite methods. In addition, the Axilrod–Teller–Muto[41,42] three-body dipole-dipole-dipole term, hereafter denoted as (ABC), is also included .

The removal of the basis set superposition error (BSSE) due to the use of small basis sets is accomplished through the geometrical counterpoise correction[29]:

$$E_{\mathrm{BSSE}}^{\mathrm{gCP}} = \frac{\sigma}{2}\sum_{AB} V_A^{\mathrm{gCP}}(R_{AB})\, f_{\mathrm{damp}}^{\mathrm{gCP}}(R_{AB}) \tag{4}$$

The difference in atomic energy between a large (nearly complete) basis set and the target basis set for each free atom is used as a measure to generate the repulsive potential $V_A^{\mathrm{gCP}}$ with fitting parameters $\alpha$, $\beta$, $\eta$.

All functional and basis set specific parameters have been optimized for each revised composite method as discussed in Ref. 33.

### B. Computational details

All the calculations have been performed with a development version of the CRYSTAL17[43,44] code, in its replicated data parallel version. For the evaluation of the DFT exchange-correlation term an XLGRID (75,974) pruned grid was used. Default convergence criterion for both energy and geometry optimization were employed. The tolerances for one- and two-electron integrals calculation were set to $10^{-7}$, $10^{-7}$ for the Coulomb and to $10^{-7}$, $10^{-7}$, $10^{-25}$ for exchange series, respectively. The shrinking factors for the diagonalization of the Hamiltonian matrix in the reciprocal space were set to 2 for the Monkhorst-Pack net and to 2 for the Gilat net respectively, except for MIL-100 and MIL-101 where the Fock matrix in the reciprocal space was diagonalized at the central point of the first Brillouin zone (i.e. $\Gamma$ point). All the properties discussed in this work have been evaluated on the fully relaxed MOFs structures (i.e. lattice parameters and atomic positions). Geometry optimization was performed with the constraints imposed by the symmetry of the system.

## III. RESULTS AND DISCUSSION

In the following, along with the results obtained with the hybrid HF/DFT composite methods, we also report data computed with the HFsol-3c method[33], for comparison. It combines HF with a minimal basis set along with the two semi-empirical terms mentioned above and a third correction for short-ranged basis incompleteness effects (see Ref.[32] for further details). As an additional comparison, present results for sol-3c methods are benchmarked against the more expensive B3LYP-D3(ABC)/pob-TZVP-rev2[45] level of theory.

### A. Equilibrium geometries

For any simulation study, obtaining reasonable structures is a mandatory starting point for further calculation such as adsorption, electronical, vibrational, and mechanical properties. This is particularly true for MOFs because of the variability of organic and inorganic building units.

Lattice parameters and bond lengths have been computed with sol-3c composite methods for a set of 15 well known MOFs (hereafter referred to as the MOF-LC15 dataset) that differ for metal ion, organic linker, topology and SBUs. Some of the crystal structures of the MOFs under examination are shown in Figure 1 (see Figures S2-S8). Results are analyzed graphically in Figure 2, which illustrates the relative percentage error of the predicted unit cell volume with respect to experimental reference data. The latter have been collected from low-temperature X-ray diffraction measurements. In addition, B3LYP-D3(ABC)/pob-TZVP-rev2 results are also shown for comparison. Detailed computed results are reported Tables S1-S6.

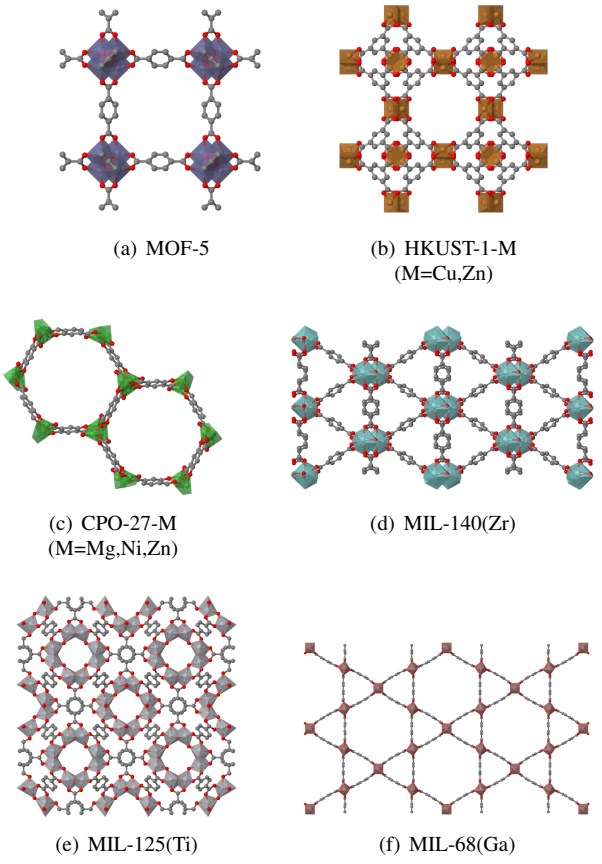

(a) MOF-5 (b) HKUST-1-M (M=Cu,Zn) (c) CPO-27-M (M=Mg,Ni,Zn) (d) MIL-140(Zr) (e) MIL-125(Ti) (f) MIL-68(Ga)

FIG. 1. Crystal structure of selected MOFs included in the MOF-LC15 dataset. The inorganic building units are represented by translucent coordination polyhedra of different colors. Color code for atoms: O in red, C in grey, Hydrogens are omitted for clarity.

PBEsol0-3c and HSEsol-3c give results similar to each other thus indicating that the screening of the HF exchange does not impact the property under consideration. They are both in excellent accord with B3LYP-D3(ABC)/pob-TZVP-rev2 results with an overall good agreement with the experimental values. Hybrid sol-3c composite methods show remarkably small relative error of $\pm 2\%$ expect for MIL-53(Al) in the narrow pore (NP) phase for which a significant underestimation of the unit cell volume is observed. This is related to the peculiar structure of MIL-53(Al) NP (vide infra) in which aromatic rings of the linkers are in close contact and dispersive contributions play a relevant role thus suggesting that the D3 correction could be partly overestimated. HFsol-3c tends to underestimate the volume of conventional cell of CPO-27-(M)[46] (M=Zn, Mg, Ni), HKUST-1(M)[47,48] (M=Zn, Cu), MIL-53(Al)[16] (NP, LP), MIL-125(Ti)[49] and UiO-66[50] dehydroxylated, while for the other systems it gives lattice parameters in reasonable agreement with the experimental data. However, it overestimates the lattice volume of MOF-5[51] and MIL-47(V)[52] with a Relative Error% (RE%) greater than 4% and 8%, respectively. This large discrepancy is probably caused by the combination of the HF method with a minimal basis set.

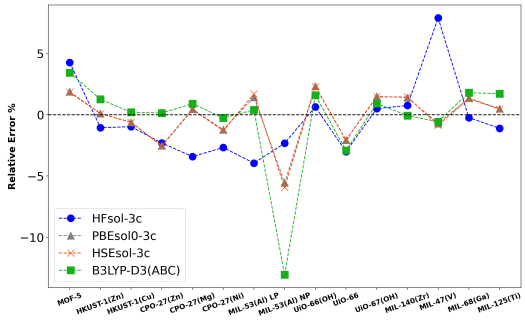


FIG. 2. Relative Error % (RE%) from experimental unit cell volumes computed at HFsol-3c, PBEsol0-3c, HSEsol-3c and B3LYP-D3(ABC)/pob-TZVP-rev2 for a dataset containing 15 well-known MOFs.

Another important structural feature for MOFs is the metal-ligand bond length that characterizes the link between the inorganic and the organic building blocks, This is particulary relevant to properly describe the structure of hybrid organic-inorganic materials as MOFs and usually quite hard to be predicted even by well-tuned force fields[53–57]. Results are gathered in Table S7-S11 of the Supporting Information. Overall, metal-ligand bonds computed with PBEsol0-3c and HSEsol-3c are in good agreement with B3LYP-D3(ABC)/pob-TZVP-rev2 data used as reference. Instead, HFsol-3c systematically underestimates the metal-linker distance for all the systems except for MIL-47(V), where a lengthening is observed. Again, this could be related to the use of a minimal basis set in the composite method.

Overall, sol-3c HF/DFT composite methods predict structures of similar quality as dispersion-corrected B3LYP with triple-zeta basis sets, or even better, but at a lower cost.

### B. Vibrational frequencies and simulated IR and Raman spectra

As an example of the ability of sol-3c methods to provide high quality vibrational frequencies and to simulate IR and Raman spectra, we selected the well-known UiO-66 Zirconium-MOF for which accurate experimental measurements are available.[50,58]

Its framework is built of $Zr_6O_4(OH)_4$ units linked by 12-fold connection through 1,4-benzene-dicarboxylate (BDC) ligands. Vibrational frequencies were computed at the $\Gamma$ point on the fully optimized structure. Infrared and Raman intensity were calculated via a linear response CPHF/KS approach as detailed in Ref.[59,60] A Lorentzian broadening of 5 $cm^{-1}$ was adopted for both the spectra. As common practice[61,62] computed vibrational frequencies were scaled for a better comparison with experimental spectra. Here, a factor of 0.95 was used. The spectra were simulated at the PBEsol0-3c level of theory.

As shown in Figure 3(a) and 3(b) for IR and Raman spectra, respectively, the overall agreement between experimental and theoretical results is excellent in both cases. This result offer an example of how composite methods can be used in supporting the experimental evidence and interpreting measured spectra. Indeed, several spectral regions may be highlighted and assigned to vibrational modes, concisely: i) the first one around 3839 $^{-1}$ related to the OH stretching of isolated hydroxyls of the inorganic cluster; ii) the second one around 3200 $^{-1}$ where CH stretching of benzene-dicarboxyl moiety are observed; iii) the third one between 1700 and 1200 $^{-1}$ characterized by bands due to asymmetric and symmetric modes of carboxylate; iv) the fourth is the region 1200-600 $^{-1}$ characterized by in-plane and out-of-plane deformation modes of aromatic rings and C-H groups; v) the fifth region (600-200 $^{-1}$) characterized by modes due to inorganic cluster deformation as the Zr-O symmetric and asymmetric vibrations and $\mu_3$-OH stretching; vi) a last interval concerns the mode below 200 $^{-1}$, where collective vibrations and lattice modes are present. Recently, the good performance of the PBEsol0-3c method in the prediction of vibrational frequencies and IR/Raman spectra has been also confirmed in the study of encapsulated molecules in HKUST-1(Cu)[63] and ZIF-8[64].

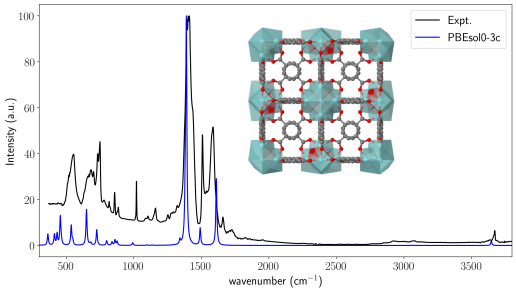


(a) UiO-66(Zr) IR spectrum

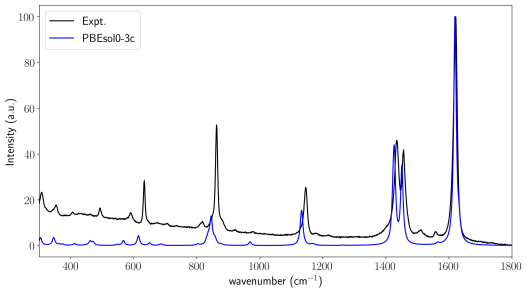


(b) UiO-66(Zr) Raman spectrum

FIG. 3. (a) Comparison between experimental and simulated (a) Infrared and (b) Raman spectra of hydroxylated UiO-66(Zr) as computed with the PBEsol0-3c composite method. Simulated Raman spectrum refers to 298.15 K with an incoming laser frequency of 785 nm. The unit cell of hydroxylated UiO-66(Zr) is also shown as inset.

### C. Fundamental band gap and dielectric constant

MOFs have also emerged as interesting materials for their electronic and dielectric properties as low band gap materials with very small dielectric constant ($k$) with promising applications as optical and optoelectronic materials.[7,20,65–69] Therefore, an accurate prediction of the band gap is important for a precise estimation of the dielectric response[8].

For this properties, HFsol-3c is not of interest because of the well-known overestimation of the band gap of the HF method, while the hybrid sol-3c composite methods have been designed with a certain percentage of exact exchange that makes them quite effective in the description of the electronic structure of solids. Figure 4 shows the fundamental band gap calculated with the hybrid HF/DFT composite methods for a series of Isoreticular Metal-Organic Frameworks (IRMOF) and other selected MOFs for which experimental data are available[70–73]. PBEsol0-3c tends to systematically overestimate the band gap for all of the systems considered as well as B3LYP-D3(ABC)/pob-TZVP-rev2. The only exception is represented by HSEsol-3c, which thanks to its screened Coulomb exchange potential gives results in very good agreement with the experimental values, in particular for UiO-66-OH-$NH_2$ and MIL-125-$NH_2$. HSEsol-3c seems to be the most promising method for describing fundamental band gap of MOFs with a Mean Absolute Relative Error % (MARE%) of 8.8% followed by B3LYP-D3(ABC) and PBEsol0-3c with a MARE% of 14.1% and 27.1% respectively (see Table S12). For PBEsol0-3c, we also computed the unit cell polarizability and the corresponding dielectric constant at the static limit. Results are reported in the supporting information (see Table S12 ). As discussed by some of us[8], the polarizability of the different frameworks largely depends on the type of ligand and topology, whereas the dielectric constant that inversely depends on the unit cell volume becomes very small and covers a range of 1.2-2.0. Present results confirm that trend with the values of $k$ being close to

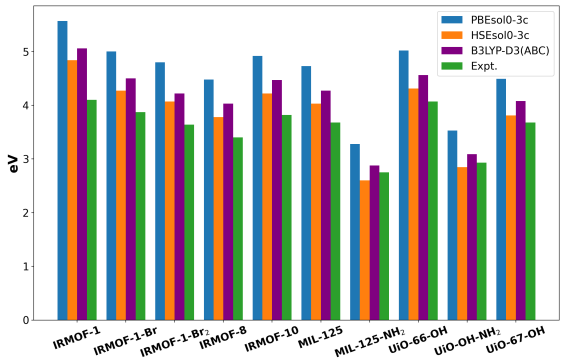


FIG. 4. Comparison between experimental value taken from Ref.[70–73] and the computed band gaps by using different level of theory.

the one computed with B3LYP-D3(ABC)/pob-TZVP-rev2.

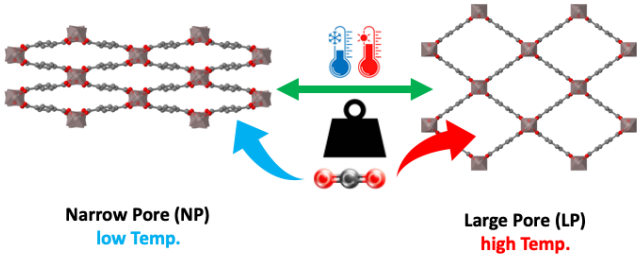


FIG. 5. Reversible switch of the MIL-53 framework between narrow-pore phase (NP) and large-pore phase (LP). This effect is mediated by external stimuli such as pressure, temperature and gas adsorption.

### D. The MIL-53(Al) bistability

MOFs are stimuli-responsive materials[74]. One of the most striking evidences of this property is the breathing behavior of the isoreticular family of MIL-53[75] and other MOFs as MIL-68 (Ga) and MIL-47 (V)[52,76]. Indeed, depending on the temperature, pressure or interaction with adsorbed gases the framework undergoes a reversible phase transition between a narrow pore (NP) structure and a large pore (LP) phase. This peculiar behaviour can be very important for selective adsorption processes[77–80] or as molecular sieve but also for tuneable dielectrics[81].
Here, we focus on the temperature-driven phase bistability of MIL-53(Al)[16,82] between the low temperature monoclinic NP structure and the high temperature orthorhombic LP one. Concerning structural parameters for both systems (see Table I for unit cell volumes and Table S3 for lattice parameters), overall results obtained with composite sol-3c methods are in reasonable agreement with the experimental values measured at 77K by neutron diffraction technique. As mentioned before, for MIL-53(Al)[16] LP, HFsol-3c yields slightly underestimated lattice parameters and volume, while the composite HF/DFT methods provide results in good agreement with the experimental data. For MIL-53(Al)[75] NP, all composite methods provide a volume that is underestimated with respect to the experimental one.

The relative stability of the two phases of MIL-53(Al) for all of the examined methods are also reported in Table I). As expected, MIL-53(Al) NP is the most stable structure at all levels of theory.

TABLE I. Unit cell volumes (in Å$^3$) of the LP and NP structures of MIL-53(Al) and electronic energy difference between the two phases (in kJ/mol).

| Method | Vol. LP | Vol. NP | $\Delta E_{lp-np}$ |
|---|---|---|---|
| HFsol-3c | 1363.1 | 843.9 | 3.9 |
| PBEsol0-3c | 1439.7 | 815.9 | 13.4 |
| HSEsol-3c | 1443.3 | 812.6 | 11.7 |
| B3LYP-D3(ABC)/VTZP[81] | 1436.5 | 802.2 | 19.4 |
| RPA+EC[83] | 1455 | 860 | 7.4 |
| Exp. (T=77K)[16] | 1419.2 | 863.9 | - |

Hybrid composite methods, in particular HSEsol-3c, provide a relative stability of the two phases close to the recently reported RPA+EC value of 7.4 kJ/mol[75,83], while HFsol-3c tends to underestimate the relative stability of the two phases.

### E. Gas adsorption

MOFs represent very promising materials for gas separation and storage thanks to the combination of high surface area with coordinatively unsaturated metal sites, which can act as Lewis acid and directly interact with the adsorbate. In this section we discuss the adsorption of two small molecules as CO and $CO_2$ on CPO-27-M (M=Mg, Zn) and HKUST-1(Cu).(see Figures S9 and S10) The calculated interaction energies are compared with the experimental values obtained from calorimetric measurements at room temperature. It is worth noting that the former should be corrected to include the zero-point vibrational energy and a thermal correction to enthalpy at the given temperature. This contribution has been estimated to be small and to amount around 3.5-5.0 kJ/mol for CPO-27(M)[84] at room temperature, therefore it has not been explicitly taken into account in the present work.
Adsorption of $CO_2$ causes a decrease of both lattice parameters and unit cell volume for all the systems herein discussed with respect to pristine material (see Tables S13, S15 and S17), The compression is greater for CPO-27(Zn) rather than HKUST-1(Cu) and CPO-27(Mg).
$CO_2$ adsorption energies calculated with composite methods are shown in Figure 6 in comparison with experimental data used as reference and B3LYP-D3(ABC)/pob-TZVP-rev2 results. HFsol-3c strongly overestimates the interaction energy while both PBEsol0-3c and HSEsol-3c give similar

results in good agreement with experiment. Interestingly, the accord would be even better when including the estimated ZPE and thermal correction to enthalpy at room temperature.

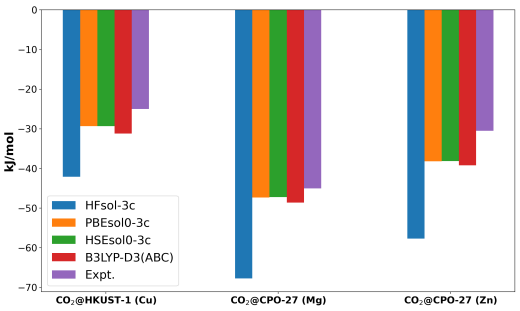


FIG. 6. Adsorption energy for $CO_2$ in HKUST-1(Cu) and CPO-27-M (M=Mg,Zn), comparison between calculated electronic energy at different level of theory and experimental heat of adsorption.

As regards the adsorption of CO, the host-guest interaction causes again a contraction of the cell with respect to the pristine material (see Tables S14, S16 and S18). The trend is similar to the adsorption of $CO_2$ with the decrease of the lattice parameters and unit cell volume being greater for CPO-27(Zn) and smaller for HKUST-1(Cu), while for CPO-27(Mg) there is no sizeable modification of the structure. At variance with $CO_2$, both HF and hybrid composite methods give a largely overestimated interaction energy between CO and the metal centre for all examined MOFs as clearly shown in Figure S11. In this case, B3LYP-D3(ABC)/pob-TZVP-rev2 results nicely agrees with experiment thus suggesting some not well balanced basis set dependence for the composite methods. Preliminary results indicates that the proper description of the interaction of CO with the adsorption site requires a more flexible basis set for carbon. Work is in progress to further check it.

We also analyzed the interatomic distance and the angle between the metal center and the adsorbed molecules (see Tables S19-S24). For CO, HFsol-3c provides both distances and angles in agreement with B3LYP-D3(ABC)/pob-TZVP-rev2 data, while PBEsol0-3c and HSEsol-3c underestimate the M—CO distance. Concerning $CO_2$, composite HF/DFT methods provides bond length in good agreement with B3LYP-D3(ABC)/pob-TZVP-rev2 data, while HFsol-3c underestimates the interaction distance. In this case, $CO_2$ forms a bent complex with MOFs that has been explained in terms of the electrostatic interaction between O atoms of the carboxylic groups around the metal and the quadrupole moment of $CO_2$[84].

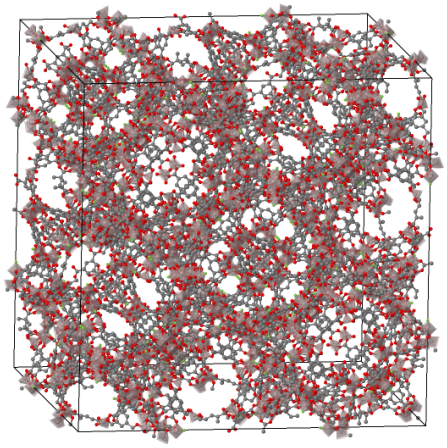

(a) MIL-100-M (M=Al,Sc,Cr,Fe)

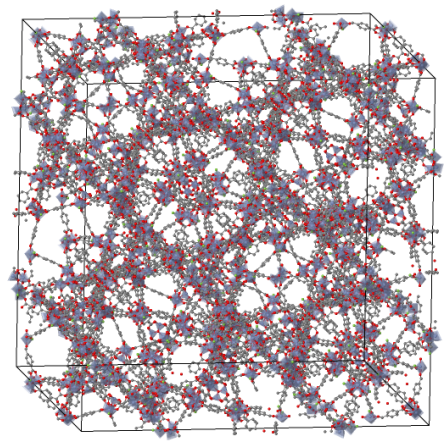

(b) MIL-101-M (M=Al,Cr)

FIG. 7. Crystallographic unit cell of (a) MIL-100-M (M=Al,Sc,Cr,Fe) and (b) MIL-101-M (M=Al,Cr). The inorganic building units are represented by translucent coordination polyhedra of different colors. Color code for atoms: O in red, C in grey, Hydrogens are omitted for clarity.

### F. Pushing the limit of sol-3c methods: Giant MOFs

In the introduction we mentioned the very large variability in the number of atoms in the unit cell of MOFs that can make the quantum-mechanical modeling very challenging. So far, we have reported and discussed results for small-to-medium MOFs with tenths-to-hundredths atoms in the unit cell. In the following, we show how "sol-3c" methods can be effectively applied to large and very large MOFs with thousands of atoms in the unit cell. In particular, we focused on the so-called giant-MOFs, namely: MIL-100 and MIL-101 (see Figure 7). They are comprised of oxo-centered trinuclear units (denoted as trimeric units or TU) of trivalent metals, namely Al and Cr, connected with 1,3,5 BTC (benzene-1,3,5-tricarboxylic acid) and 1,4 BDC (benzene-1,4-dicarboxylic acid), respectively. Starting from the experimental cubic crystalline structure of MIL-100 and MIL-101 we removed all water molecules and positioned a counterion on one of the metal of each TU. For sake of simplicity, we decided to model MIL-100 and MIL-

TABLE II. Predicted lattice parameters and unit cell volumes of MIL-100 ($M^{III}$) optimized at HFsol-3c, PBEsol0-3c and HSEsol-3c level of theory in comparison with B3LYP-D*/TZVP[85] results and experimental data[86–89] along with percentage deviation of unit cell volume (ΔV%)

| $Al^{III}$ | a(Å) | c(Å) | c/a | volume(Å$^3$) | mean LP(Å) | ΔV% |
|---|---|---|---|---|---|---|
| HFsol-3c | 70.701 | 70.563 | 0.9980 | 352723.1 | 70.655 | -4.26 |
| PBEsol0-3c | 71.484 | 71.284 | 0.9972 | 364258.7 | 71.417 | -1.12 |
| HSEsol-3c | 71.462 | 71.262 | 0.9972 | 363922.8 | 71.395 | -1.22 |
| B3LYP-D*/TZVP[85] | 71.531 | 71.494 | 0.9995 | 365813.0 | 71.519 | -0.70 |
| Exp.[86] | 71.678 | - | - | 368401.0 | - | - |
| $Sc^{III}$ | a(Å) | c(Å) | c/a | volume(Å$^3$) | mean LP(Å) | ΔV% |
| HFsol-3c | 73.990 | 74.051 | 1.001 | 405390.7 | 74.010 | -1.37 |
| PBEsol0-3c | 74.283 | 74.319 | 1.000 | 410090.8 | 74.295 | -0.22 |
| HSEsol-3c | 74.270 | 74.280 | 1.000 | 409732.7 | 74.273 | -0.31 |
| B3LYP-D*/TZVP[85] | 74.676 | 74.823 | 1.002 | 417248.2 | 74.725 | 1.52 |
| Exp.[87] | 74.350 | - | - | 411001.0 | - | - |
| $Cr^{III}$ | a(Å) | c(Å) | c/a | volume(Å$^3$) | mean LP(Å) | ΔV% |
| HFsol-3c | 72.410 | 72.452 | 1.001 | 379876.3 | 72.424 | -1.97 |
| PBEsol0-3c | 72.470 | 72.497 | 1.000 | 380749.0 | 72.479 | -1.75 |
| HSEsol-3c | 72.456 | 72.479 | 1.000 | 380503.3 | 72.464 | -1.81 |
| B3LYP-D*/TZVP[85] | 72.602 | 73.249 | 1.009 | 386097.1 | 72.818 | -0.36 |
| Exp.[88] | 72.906 | - | - | 387511.4 | - | - |
| $Fe^{III}$ | a(Å) | c(Å) | c/a | volume(Å$^3$) | mean LP(Å) | ΔV% |
| HFsol-3c | 72.677 | 72.738 | 1.001 | 384197.7 | 72.697 | -2.61 |
| PBEsol0-3c | 72.940 | 72.724 | 0.997 | 386913.6 | 72.868 | -1.92 |
| HSEsol-3c | 72.919 | 72.712 | 0.997 | 386622.8 | 72.850 | -1.99 |
| B3LYP-D*/TZVP[85] | 73.158 | 73.302 | 1.002 | 392311.9 | 73.206 | -0.55 |
| Exp.[89] | 73.340 | - | - | 394481.1 | - | - |

101 with fluoride as counterion to save as many symmetry operators as possible. The final model structures result in a tetragonal space group that still retains 16 symmetry operators with primitive unit cells containing about 2800 and 3600 atoms, respectively.

In Table II we report the optimized lattice parameters and unit cell volume for MIL-100 computed with sol-3c composite methods along with experimental data and B3LYP-D*/TZVP results (hereafter we use TZVP as shortcut for the combination of pob-TZVP and 6-311G(d,p) basis sets) taken from Ref[85] Although the computed unit cell is tetragonal, the difference between $a$ and $c$ parameters is very small with the $c/a$ ratio being close to one. Therefore, a very small deviation from cubic lattice is predicted for MIL-100 so that the optimized structures can be considered as pseudo-cubic, with a mean lattice parameter remarkably close to the experimental values. The overall structural results obtained with our sol-3c methods are consistent with both B3LYP-D*/TZVP calculations and experimental data, in particular the DFT composite methods provide a percentage deviation of the unit cell volume from experimental data below 1.5%, while HFsol-3c shows a slightly larger deviation of about 4.2%.

The same excellent agreement is also obtained for the even larger MOF MIL-101, as reported in Table III. Experimental data are available solely for MIL-101(Cr) for comparison. For lattice constant and volume a remarkable accord with predicted results is observed. A similar correspondence is obtained for MIL-101(Al), too, but in this case the lattice parameters has been estimated by considering the similarity between the structure of MIL-100 and MIL-101 and scaling the volume of MIL-101(Cr) with the ratio of the volumes of MIL-100(Cr) and MIL-100(Al).

Overall, present results for giant-MOFs are quite striking if one considers the size and complexity of those systems. Furthermore, it is worth noting that B3LYP-D*/TZVP calculations on MIL-100 required supercomputing resources with 1024 CPU cores, at least, whereas with hybrid sol-3c methods a full relaxation of the structures can be easily carried out on just 60 CPU cores in less than a week[90]. Therefore, accurate large-scale calculations become affordable on small-to-medium computing resources that are commonly available in many research laboratories[34].

## IV. CONCLUSIONS

In this work, we reported on the application of a family of ab initio composite methods designed for solid-state calculations to study several properties of Metal-Organic Frameworks.

In particular, we focused on composite methods based on hybrid density functional approximations. The combination of both global and range-separated hybrid functionals as PBEsol0 and HSEsol, combined with a double-zeta quality basis set and augmented with properly tuned semi-classical corrections turns out to be quite effective and reliable in modelling MOFs. They show a remarkably good performance in predicting structures, band gaps, vibrational frequencies and partly adsorption energies.

We also benchmarked the simpler HFsol-3c composite

TABLE III. Predicted LPs of MIL-101 ($M^{III}$) optimized at HFsol-3c, PBEsol0-3c and HSEsol-3c level of theory in comparison with experimental data[91] along with percentage deviation of unit cell volume (ΔV%)

| $Al^{III}$ | a(Å) | c(Å) | c/a | volume(Å$^3$) | mean LP(Å) | ΔV% |
|---|---|---|---|---|---|---|
| HFsol-3c | 86.514 | 86.588 | 1.0009 | 648082.8 | 86.539 | -2.87 |
| PBEsol0-3c | 87.464 | 87.497 | 1.0004 | 669341.9 | 87.475 | 0.31 |
| HSEsol-3c | 87.442 | 87.476 | 1.0004 | 668858.8 | 87.454 | 0.24 |
| Exp.[a] | 87.383 | - | - | 667247.6 | - | - |
| $Cr^{III}$ | a(Å) | c(Å) | c/a | volume(Å$^3$) | mean LP(Å) | ΔV% |
| HFsol-3c | 88.677 | 88.684 | 1.0001 | 697374.4 | 88.679 | -0.64 |
| PBEsol0-3c | 88.843 | 88.792 | 0.9994 | 700848.0 | 88.826 | -0.14 |
| HSEsol-3c | 88.821 | 88.772 | 0.9994 | 700340.0 | 88.805 | -0.22 |
| Exp[91]. | 88.869 | - | - | 701860.3 | - | - |

[a] Estimated values, see text for details.

method. Although it shows some drawbacks due to the limitation of the Hartree-Fock method combined with a minimal basis set, the smaller computational cost makes it promising for either high-throughput screening of MOFs or as an entry level for very large-scale calculations on MOFs that contain thousands of atoms in the unit cell.

Overall, hybrid sol-3c composite methods provide results of comparable or with even better quality than the more demanding B3LYP-D3(ABC)/pob-TZVP-rev2 method. As an example, the cost of a single SCF cycle and gradient calculation for MIL-127(Al) a MOF with more than 400 atoms in the unit cell and 8 symmetry operators, is 1.5-2.0 times larger than the hybrid sol-3c composite methods (see Fig.s S12-S13). This proves that they are of practical use also for complex solids as MOFs. Furthermore, the effective deploy of hybrid functionals reduces the delocalization error that plagues DFT approximations in solid state calculations, in particular when transition metals are involved.

We are confident that hybrid sol-3c composite methods are valuable and cost-effective computational tools for MOFs and can be used for In Silico prediction of properties beyond plain structural features[92].

## CONFLICTS OF INTEREST

There are no conflicts of interest to declare.

## ACKNOWLEDGMENTS

L.D and B.C would like to thank Dr. Francesca Bonino for sharing the experimental IR and Raman spectra of UiO-66(OH) and for helpful discussions.

## SUPPLEMENTARY MATERIAL

See Supplementary Material for: lattice parameters, conventional cell volumes, metal-linker bond lengths and additional figures of the MOFs in the MOF-LC15 dataset; fundamental band gaps, unit cell polarizabilities and dielectric constants of selected MOFs; conventional cell parameters, metal-linker bond lengths, adsorption energies and figures of CO and $CO_2$ adsorbed in CPO-27(M) (Mg,Zn) and HKUST-1(Cu); cost efficiency methods comparison for MIL-127(Al).

[1] Jeffrey R Long and Omar M Yaghi. The pervasive chemistry of metal–organic frameworks. *Chemical Society Reviews*, 38(5):1213–1214, 2009.

[2] Stuart R Batten, Neil R Champness, Xiao-Ming Chen, Javier Garcia-Martinez, Susumu Kitagawa, Lars Öhrström, Michael O'Keeffe, Myunghyun Paik Suh, and Jan Reedijk. Terminology of metal–organic frameworks and coordination polymers (iupac recommendations 2013). *Pure and Applied Chemistry*, 85(8):1715–1724, 2013.

[3] Shengqian Ma and Hong-Cai Zhou. Gas storage in porous metal–organic frameworks for clean energy applications. *Chemical Communications*, 46(1):44–53, 2010.

[4] Hao Li, Kecheng Wang, Yujia Sun, Christina T Lollar, Jialuo Li, and Hong-Cai Zhou. Recent advances in gas storage and separation using metal–organic frameworks. *Materials Today*, 21(2):108–121, 2018.

[5] MA Nasalevich, M Van der Veen, F Kapteijn, and J Gascon. Metal–organic frameworks as heterogeneous photocatalysts: advantages and challenges. *CrystEngComm*, 16(23):4919–4926, 2014.

[6] Pawan Kumar, Akash Deep, and Ki-Hyun Kim. Metal organic frameworks for sensing applications. *TrAC Trends in Analytical Chemistry*, 73:39–53, 2015.

[7] Vitalie Stavila, A Alec Talin, and Mark D Allendorf. Mof-based electronic and opto-electronic devices. *Chemical Society Reviews*, 43(16):5994–6010, 2014.

[8] Matthew R Ryder, Lorenzo Donà, Jenny G Vitillo, and Bartolomeo Civalleri. Understanding and controlling the dielectric response of metal–organic frameworks. *ChemPlusChem*, 83(4):308–316, 2018.

[9] Patricia Horcajada, Tamim Chalati, Christian Serre, Brigitte Gillet, Catherine Sebrie, Tarek Baati, Jarrod F Eubank, Daniela Heurtaux, Pascal Clayette, Christine Kreuz, et al. Porous metal–organic-framework nanoscale carriers as a potential platform for drug delivery and imaging. *Nature materials*, 9(2):172–178, 2010.

[10] Patricia Horcajada, Christian Serre, María Vallet-Regí, Muriel Sebban, Francis Taulelle, and Gérard Férey. Metal–organic frameworks as efficient materials for drug delivery. *Angewandte chemie*, 118(36):6120–6124, 2006.

[11] Yasuhide AU Inokuma, Shota Yoshioka, Junko Ariyoshi, Tatsuhiko Arai, Yuki Hitora, Kentaro Takada, Shigeki Matsunaga, Kari Rissanen, and Makoto Fujita. X-ray analysis on the nanogram to microgram scale using porous complexes. *Nature*, 495:461–466, 2013.

[12] See https://www.merckgroup.com/en/research/innovation-center/highlights/crystallinesponge.html.

[13] Peyman Z Moghadam, Aurelia Li, Seth B Wiggin, Andi Tao, Andrew GP Maloney, Peter A Wood, Suzanna C Ward, and David Fairen-Jimenez. Development of a cambridge structural database subset: a collection of metal–organic frameworks for past, present, and future. *Chemistry of Materials*, 29(7):2618–2625, 2017.

[14]Peyman Z Moghadam, Aurelia Li, Xiao-Wei Liu, Rocio Bueno-Perez, Shu-Dong Wang, Seth B Wiggin, Peter A Wood, and David Fairen-Jimenez. Targeted classification of metal–organic frameworks in the cambridge structural database (csd). *Chemical science*, 11(32):8373–8387, 2020.

[15]Yongchul G. Chung, Emmanuel Haldoupis, Benjamin J. Bucior, Maciej Haranczyk, Seulchan Lee, Hongda Zhang, Konstantinos D. Vogiatzis, Marija Milisavljevic, Sanliang Ling, Jeffrey S. Camp, Ben Slater, J. Ilja Siepmann, David S. Sholl, and Randall Q. Snurr. Advances, updates, and analytics for the computation-ready, experimental metal–organic framework database: Core mof 2019. *Journal of Chemical & Engineering Data*, 64(12):5985–5998, 2019.

[16]Y. Liu, J. Her, A. Dailly, A. J. Ramirez-Cuesta, D. Neumann, and C. M. Brown. Reversible structural transition in mil-53 with large temperature hysteresis. *J. Am. Chem. Soc.*, 130:11813–11818, 2008.

[17]G. Férey, C. Serre, C. Mellot-Draznieks, F. Millange, S. Surblé, J. Dutour, and I. Margiolaki. A hybrid solid with giant pores prepared by a combination of targeted chemistry, simulation, and powder diffraction. *Angew. Chem. Int. Ed.*, 43:6296–6301, 2004.

[18]Jihyun An, Omar K Farha, Joseph T Hupp, Ehmke Pohl, Joanne I Yeh, and Nathaniel L Rosi. Metal-adeninate vertices for the construction of an exceptionally porous metal-organic framework. *Nature communications*, 3(1):1–6, 2012.

[19]Tao Li, Mark T Kozlowski, Evan A Doud, Maike N Blakely, and Nathaniel L Rosi. Stepwise ligand exchange for the preparation of a family of mesoporous mofs. *Journal of the American Chemical Society*, 135(32):11688–11691, 2013.

[20]Jenna L Mancuso, Austin M Mroz, Khoa N Le, and Christopher H Hendon. Electronic structure modeling of metal–organic frameworks. *Chemical Reviews*, 120(16):8641–8715, 2020.

[21]R. Sure and S. Grimme. Corrected small basis set Hartree-Fock method for large systems. *J. Comp. Chem.*, 34:1672–1685, 2013.

[22]S. Grimme, J. G. Brandenburg, C. Bannwarth, and A. Hansen. Consistent structures and interactions by density functional theory with small atomic orbital basis sets. *J. Chem. Phys.*, 143:054107, 2015.

[23]J. G. Brandenburg, E. Caldeweyher, and S. Grimme. Screened exchange hybrid density functional for accurate and efficient structures and interaction energies. *Phys. Chem. Chem. Phys.*, 18:15519–15523, 2016.

[24]J. G. Brandenburg, C. Bannwarth, A. Hansen, and S. Grimme. B97-3c: A revised low-cost variant of the B97-D density functional method. *J. Chem. Phys.*, 148:064104, 2018.

[25]Stefan Grimme, Andreas Hansen, Sebastian Ehlert, and Jan-Michael Mewes. r2scan-3c: An efficient "swiss army knife" composite electronic-structure method. 2020.

[26]Stefan Grimme, Jens Antony, Stephan Ehrlich, and Helge Krieg. A consistent and accurate ab initio parametrization of density functional dispersion correction (dft-d) for the 94 elements h-pu. *The Journal of chemical physics*, 132(15):154104, 2010.

[27]E. Caldeweyher, C. Bannwarth, and S. Grimme. Extension of the d3 dispersion coefficient model. *J. Chem. Phys.*, 147(034112), 2017.

[28]Eike Caldeweyher, Jan-Michael Mewes, Sebastian Ehlert, and Stefan Grimme. Extension and evaluation of the D4 London-dispersion model for periodic systems. *Phys. Chem. Chem. Phys.*, 22(16):8499–8512, 2020.

[29]H. Kruse and S. Grimme. A geometrical correction for the inter-and intramolecular basis set superposition error in Hartree-Fock and density functional theory calculations for large systems. *J. Chem. Phys.*, 136:154101, 2012.

[30]J. G. Brandenburg, M. Alessio, B. Civalleri, M. F. Peintinger, T. Bredow, and S. Grimme. Geometrical correction for the inter-and intramolecular basis set superposition error in periodic density functional theory calculations. *J. Phys. Chem. A*, 117:9282–9292, 2013.

[31]Gregory J. O. Beran. Modeling polymorphic molecular crystals with electronic structure theory. *Chemical Reviews*, 116(9):5567–5613, 2016.

[32]E. Caldeweyher and J. G. Brandenburg. Simplified DFT methods for consistent structures and energies of large systems. *J. Phys.: Condens. Matter*, 30:213001, 2018.

[33]L. Doná, J. G. Brandenburg, and B. Civalleri. Extending and assessing composite electronic structure methods to the solid state. *J. Chem. Phys.*, 151:121101, 2019.

[34]L Donà, JG Brandenburg, IJ Bush, and B Civalleri. Cost-effective composite methods for large-scale solid-state calculations. *Faraday Discussions*, 224:292–308, 2020.

[35]OI Lebedev, F Millange, C Serre, G Van Tendeloo, and G Férey. First direct imaging of giant pores of the metal- organic framework mil-101. *Chemistry of materials*, 17(26):6525–6527, 2005.

[36]J. P. Perdew, A. Ruzsinszky, G. I. Csonka, O. A. Vydrov, G. E. Scuseria, L. A. Constantin, X. Zhou, and K. Burke. Restoring the density-gradient expansion for exchange in solids and surfaces. *Phys. Rev. Lett.*, 100:136406, 2008.

[37]L. Schimka, J. Harl, and G. Kresse. Improved hybrid functional for solids: The HSEsol functional. *J. Chem. Phys.*, 134:024116, 2011.

[38]C. Adamo and V. Barone. Toward reliable density functional methods without adjustable parameters: The pbe0 model. *J. Chem. Phys.*, 110:6158–6170, 1999.

[39]E. R. Johnson and A. D. Becke. A post-hartree-fock model of intermolecular interactions: Inclusion of higher-order corrections. *J. Chem. Phys.*, 124:174104, 2006.

[40]S. Grimme, S. Ehrlich, and L. Goerigk. Effect of the damping function in dispersion corrected density functional theory. *J. Comp. Chem.*, 32:1456–1465, 2011.

[41]B. M. Axilrod and E. Teller. Interaction of the van der Waals type between three atoms. *J. Chem. Phys.*, 11:299–300, 1943.

[42]Y. Muto. Force between nonpolar molecules. *J. Phys. Math. Soc. Jpn*, 17:629–631, 1943.

[43]R. Dovesi, A. Erba, R. Orlando, C. M. Zicovich-Wilson, B. Civalleri, L. Maschio, M. Rérat, S. Casassa, J. Baima, S. Salustro, et al. Quantum-mechanical condensed matter simulations with CRYSTAL. *WIREs Comput Mol Sci.*, 8:e1360, 2018.

[44]A. Erba, J. Baima, I. Bush, R. Orlando, and R. Dovesi. Large-scale condensed matter dft simulations: Performance and capabilities of the crystal code. *J. Chem. Theory Comput.*, 13:5019–5027, 2017.

[45]Daniel Vilela Oliveira, Joachim Laun, Michael F Peintinger, and Thomas Bredow. Bsse-correction scheme for consistent gaussian basis sets of double-and triple-zeta valence with polarization quality for solid-state calculations. *Journal of computational chemistry*, 40(27):2364–2376, 2019.

[46]N. L Rosi, J. Kim, M. Eddaoudi, B. Chen, M. O'Keeffe, and O. M. Yaghi. Rod packings and metal- organic frameworks constructed from rod-shaped secondary building units. *J. Am. Chem. Soc.*, 127:1504–1518, 2005.

[47]H. Furukawa, K. E. Cordova, M. O'Keeffe, and O. M. Yaghi. The chemistry and applications of metal-organic frameworks. *Science*, 341:1230444, 2013.

[48]Manas K Bhunia, James T Hughes, James C Fettinger, and Alexandra Navrotsky. Thermochemistry of paddle wheel mofs: Cu-hkust-1 and zn-hkust-1. *Langmuir*, 29(25):8140–8145, 2013.

[49]Meenakshi Dan-Hardi, Christian Serre, Théo Frot, Laurence Rozes, Guillaume Maurin, Clément Sanchez, and Gérard Férey. A new photoactive crystalline highly porous titanium (iv) dicarboxylate. *Journal of the American Chemical Society*, 131(31):10857–10859, 2009.

[50]J. H. Cavka, S. Jakobsen, U. Olsbye, N. Guillou, C. Lamberti, S. Bordiga, and K. P. Lillerud. A new zirconium inorganic building brick forming metal organic frameworks with exceptional stability. *J. Am. Chem. Soc.*, 130:13850–13851, 2008.

[51]Nathaniel L Rosi, Juergen Eckert, Mohamed Eddaoudi, David T Vodak, Jaheon Kim, Michael O'Keeffe, and Omar M Yaghi. Hydrogen storage in microporous metal-organic frameworks. *Science*, 300(5622):1127–1129, 2003.

[52]Karin Barthelet, Jérôme Marrot, Didier Riou, and Gérard Férey. A breathing hybrid organic–inorganic solid with very large pores and high magnetic characteristics. *Angewandte Chemie*, 114(2):291–294, 2002.

[53]Jessica K Bristow, Jonathan M Skelton, Katrine L Svane, Aron Walsh, and Julian D Gale. A general forcefield for accurate phonon properties of metal–organic frameworks. *Physical Chemistry Chemical Physics*, 18(42):29316–29329, 2016.

[54]Derya Dokur and Seda Keskin. Effects of force field selection on the computational ranking of mofs for co2 separations. *Industrial & engineering chemistry research*, 57(6):2298–2309, 2018.

[55]Damien E Coupry, Matthew A Addicoat, and Thomas Heine. Extension of the universal force field for metal–organic frameworks. *Journal of Chemical Theory and Computation*, 12(10):5215–5225, 2016.

[56]Maxim Tafipolsky, Saeed Amirjalayer, and Rochus Schmid. Atomistic theoretical models for nanoporous hybrid materials. *Microporous and Meso-*

*porous Materials*, 129:304–318, 2010.

[57]Louis Vanduyfhuys, Steven Vandenbrande, Jelle Wieme, Michel Waroquier, Toon Verstraelen, and Veronique Van Speybroeck. Extension of the quickff force field protocol for an improved accuracy of structural, vibrational, mechanical and thermal properties of metal–organic frameworks. *Journal of Computational Chemistry*, 39(16):999–1011, 2018.

[58]Sachin Chavan, Jenny G Vitillo, Mohammed J Uddin, Francesca Bonino, Carlo Lamberti, Elena Groppo, Karl-Petter Lillerud, and Silvia Bordiga. Functionalization of uio-66 metal- organic framework and highly cross-linked polystyrene with cr (co) 3: In situ formation, stability, and photoreactivity. *Chemistry of Materials*, 22(16):4602–4611, 2010.

[59]Lorenzo Maschio, Bernard Kirtman, Roberto Orlando, and Michel Rèrat. Ab initio analytical infrared intensities for periodic systems through a coupled perturbed hartree-fock/kohn-sham method. *The Journal of chemical physics*, 137(20):204113, 2012.

[60]Lorenzo Maschio, Bernard Kirtman, Michel Rérat, Roberto Orlando, and Roberto Dovesi. Ab initio analytical raman intensities for periodic systems through a coupled perturbed hartree-fock/kohn-sham method in an atomic orbital basis. i. theory. *The Journal of chemical physics*, 139(16):164101, 2013.

[61]Anthony P Scott and Leo Radom. Harmonic vibrational frequencies: an evaluation of hartree- fock, møller- plesset, quadratic configuration interaction, density functional theory, and semiempirical scale factors. *The Journal of Physical Chemistry*, 100(41):16502–16513, 1996.

[62]Jeffrey P Merrick, Damian Moran, and Leo Radom. An evaluation of harmonic vibrational frequency scale factors. *The Journal of Physical Chemistry A*, 111(45):11683–11700, 2007.

[63]Barbara E Souza, Lorenzo Donà, Kirill Titov, Paolo Bruzzese, Zhixin Zeng, Yang Zhang, Arun S Babal, Annika F Möslein, Mark D Frogley, Magda Wolna, et al. Elucidating the drug release from metal–organic framework nanocomposites via in situ synchrotron microspectroscopy and theoretical modeling. *ACS applied materials & interfaces*, 12(4):5147–5156, 2020.

[64]Tao Xiong, Yang Zhang, Lorenzo Donà, Mario Gutiérrez, Annika F Möslein, Arun S Babal, Nader Amin, Bartolomeo Civalleri, and Jin-Chong Tan. Tunable fluorescein-encapsulated zeolitic imidazolate framework-8 nanoparticles for solid-state lighting. *ACS Applied Nano Materials*, 2021.

[65]Muhammad Usman, Shruti Mendiratta, and Kuang-Lieh Lu. Metal–organic frameworks: new interlayer dielectric materials. *ChemElectroChem*, 2(6):786–788, 2015.

[66]Shruti Mendiratta, Cheng-Hua Lee, Muhammad Usman, and Kuang-Lieh Lu. Metal–organic frameworks for electronics: emerging second order nonlinear optical and dielectric materials. *Science and technology of advanced materials*, 16(5):054204, 2015.

[67]Ekaterina A Dolgopolova and Natalia B Shustova. Metal–organic framework photophysics: Optoelectronic devices, photoswitches, sensors, and photocatalysts. *MRS Bulletin*, 41(11):890–896, 2016.

[68]Ivo Stassen, Nicholas Burtch, Alec Talin, Paolo Falcaro, Mark Allendorf, and Rob Ameloot. An updated roadmap for the integration of metal–organic frameworks with electronic devices and chemical sensors. *Chemical Society Reviews*, 46(11):3185–3241, 2017.

[69]Keith T Butler, Christopher H Hendon, and Aron Walsh. Electronic chemical potentials of porous metal–organic frameworks. *Journal of the American Chemical Society*, 136(7):2703–2706, 2014.

[70]Jorge Gascon, María D Hernández-Alonso, Ana Rita Almeida, Gerard PM van Klink, Freek Kapteijn, and Guido Mul. Isoreticular mofs as efficient photocatalysts with tunable band gap: an operando ftir study of the photoinduced oxidation of propylene. *ChemSusChem: Chemistry & Sustainability Energy & Materials*, 1(12):981–983, 2008.

[71]Christopher H Hendon, Davide Tiana, Marc Fontecave, Clément Sanchez, Loïc D'arras, Capucine Sassoye, Laurence Rozes, Caroline Mellot-Draznieks, and Aron Walsh. Engineering the optical response of the titanium-mil-125 metal–organic framework through ligand functionalization. *Journal of the American Chemical Society*, 135(30):10942–10945, 2013.

[72]Espen Flage-Larsen, Arne Røyset, Jasmina Hafizovic Cavka, and Knut Thorshaug. Band gap modulations in uio metal–organic frameworks. *The Journal of Physical Chemistry C*, 117(40):20610–20616, 2013.

[73]Sachin Chavan, Jenny G Vitillo, Diego Gianolio, Olena Zavorotynska, Bartolomeo Civalleri, Søren Jakobsen, Merete H Nilsen, Loredana Valenzano, Carlo Lamberti, Karl Petter Lillerud, et al. H 2 storage in isostructural uio-67 and uio-66 mofs. *Physical Chemistry Chemical Physics*, 14(5):1614–1626, 2012.

[74]François-Xavier Coudert. Responsive metal–organic frameworks and framework materials: Under pressure, taking the heat, in the spotlight, with friends. *Chemistry of Materials*, 27(6):1905–1916, 2015.

[75]Alexander EJ Hoffman, Jelle Wieme, Sven MJ Rogge, Louis Vanduyfhuys, and Veronique Van Speybroeck. The impact of lattice vibrations on the macroscopic breathing behavior of mil-53 (al). *Zeitschrift für Kristallographie-Crystalline Materials*, 234(7-8):529–545, 2019.

[76]Christophe Volkringer, Mohamed Meddouri, Thierry Loiseau, Nathalie Guillou, Jerome Marrot, Gerard Ferey, Mohamed Haouas, Francis Taulelle, Nathalie Audebrand, and Michel Latroche. The kagomé topology of the gallium and indium metal-organic framework types with a mil-68 structure: synthesis, xrd, solid-state nmr characterizations, and hydrogen adsorption. *Inorganic chemistry*, 47(24):11892–11901, 2008.

[77]Fabrice Salles, Aziz Ghoufi, Guillaume Maurin, Robert G Bell, Caroline Mellot-Draznieks, and Gérard Férey. Molecular dynamics simulations of breathing mofs: Structural transformations of mil-53 (cr) upon thermal activation and co2 adsorption. *Angewandte Chemie International Edition*, 47(44):8487–8491, 2008.

[78]NA Ramsahye, Guillaume Maurin, Sandrine Bourrelly, PL Llewellyn, C Serre, T Loiseau, T Devic, and G Ferey. Probing the adsorption sites for co2 in metal organic frameworks materials mil-53 (al, cr) and mil-47 (v) by density functional theory. *The Journal of Physical Chemistry C*, 112(2):514–520, 2008.

[79]David S Coombes, Furio Corà, Caroline Mellot-Draznieks, and Robert G Bell. Sorption-induced breathing in the flexible metal organic framework crmil-53: force-field simulations and electronic structure analysis. *The Journal of Physical Chemistry C*, 113(2):544–552, 2009.

[80]François-Xavier Coudert, Aurélie U Ortiz, Volker Haigis, David Bousquet, Alain H Fuchs, Anthony Ballandras, Guy Weber, Igor Bezverkhyy, Nicolas Geoffroy, Jean-Pierre Bellat, et al. Water adsorption in flexible gallium-based mil-53 metal–organic framework. *The Journal of Physical Chemistry C*, 118(10):5397–5405, 2014.

[81]Kirill Titov, Zhixin Zeng, Matthew R. Ryder, Abhijeet K. Chaudhari, Bartolomeo Civalleri, Chris S. Kelley, Mark D. Frogley, Gianfelice Cinque, and Jin-Chong Tan. Probing dielectric properties of metal–organic frameworks: Mil-53(al) as a model system for theoretical predictions and experimental measurements via synchrotron far- and mid-infrared spectroscopy. *The Journal of Physical Chemistry Letters*, 8(20):5035–5040, 10 2017.

[82]Andrew M Walker, Bartolomeo Civalleri, Ben Slater, Caroline Mellot-Draznieks, Furio Corà, Claudio M Zicovich-Wilson, Guillermo Román-Pérez, José M Soler, and Julian D Gale. Flexibility in a metal–organic framework material controlled by weak dispersion forces: the bistability of mil-53 (al). *Angewandte Chemie Int. Ed.*, 122(41):7663–7665, 2010.

[83]Jelle Wieme, Kurt Lejaeghere, Georg Kresse, and Veronique Van Speybroeck. Tuning the balance between dispersion and entropy to design temperature-responsive flexible metal-organic frameworks. *Nature communications*, 9(1):1–10, 2018.

[84]Loredana Valenzano, Bartolomeo Civalleri, Kaido Sillar, and Joachim Sauer. Heats of adsorption of co and co2 in metal–organic frameworks: quantum mechanical study of cpo-27-m (m= mg, ni, zn). *The Journal of Physical Chemistry C*, 115(44):21777–21784, 2011.

[85]Maddalena D'Amore, Bartolomeo Civalleri, Ian J Bush, Elisa Albanese, and Matteo Ferrabone. Elucidating the interaction of co2 in the giant metal–organic framework mil-100 through large-scale periodic ab initio modeling. *The Journal of Physical Chemistry C*, 123(47):28677–28687, 2019.

[86]Christophe Volkringer, Dimitry Popov, Thierry Loiseau, Gérard Férey, Manfred Burghammer, Christian Riekel, Mohamed Haouas, and Francis Taulelle. Synthesis, single-crystal x-ray microdiffraction, and nmr characterizations of the giant pore metal-organic framework aluminum trimesate mil-100. *Chemistry of Materials*, 21(24):5695–5697, 2009.

[87]LI Yan-Tao CUI Ke-Hui, LI Jia ZHU Jian-Qi WANG, and Xin TIAN Yun-Qi. The giant pore metal-organic frameworks of scandium carboxylate with mil-100 and mil-101 structures [j]. *Chinese Journal of Inorganic Chemistry*, 5, 2011.

[88]Gérard Férey, Christian Serre, Caroline Mellot-Draznieks, Franck Millange, Suzy Surblé, Julien Dutour, and Irène Margiolaki. A hybrid solid with giant pores prepared by a combination of targeted chemistry, simulation, and powder diffraction. *Angewandte Chemie*, 116(46):6456–6461,

2004.

[89] Patricia Horcajada, Suzy Surblé, Christian Serre, Do-Young Hong, You-Kyong Seo, Jong-San Chang, Jean-Marc Grenèche, Irene Margiolaki, and Gérard Férey. Synthesis and catalytic properties of mil-100 (fe), an iron (iii) carboxylate with large pores. *Chemical Communications*, (27):2820–2822, 2007.

[90] For instance, by starting from the B3LYP-D*/TZVP optimized geometry, the full relaxation of MIL-100(Cr) takes about 30 steps with a total wall-clock time of 3 days.

[91] Gerard Férey, Caroline Mellot-Draznieks, Christian Serre, Franck Millange, Julien Dutour, Suzy Surblé, and Irena Margiolaki. A chromium terephthalate-based solid with unusually large pore volumes and surface area. *Science*, 309(5743):2040–2042, 2005.

[92] Mark D. Allendorf, Vitalie Stavila, Matthew Witman, Carl K. Brozek, and Christopher H. Hendon. What lies beneath a metal–organic framework crystal structure? new design principles from unexpected behaviors. *Journal of the American Chemical Society*, 143:6705–6723, 2021.